INSTITUTE OF PHYSICS PUBLISHING CLASSICAL AND QUANTUM GRAVITY

Class. Quantum Grav. **19** (2002) 897–917 PII: S0264-9381(02)31215-2

Thermal noise in interferometric gravitational wave detectors due to dielectric optical coatings

Gregory M Harry[1,2], Andri M Gretarsson[2], Peter R Saulson[2], Scott E Kittelberger[2], Steven D Penn[2], William J Startin[2], Sheila Rowan[3], Martin M Fejer[3], D R M Crooks[4], Gianpietro Cagnoli[4], Jim Hough[4] and Norio Nakagawa[5]

[1] LIGO Laboratory, Massachusetts Institute of Technology, Room NW17-161, 175 Albany Street, Cambridge, MA 02139, USA
[2] Department of Physics, Syracuse University, Syracuse, NY 13244-1130, USA
[3] Edward L. Ginzton Lab, Stanford University, Stanford, CA 94305-4085, USA
[4] Department of Physics and Astronomy, University of Glasgow, Glasgow G12 8QQ, UK
[5] Center for Nondestructive Evaluation, Institute for Physical Research and Technology, Iowa State University, Ames, IA 50011, USA

E-mail: gharry@ligo.mit.edu and andri@physics.syr.edu

Received 26 November 2001
Published 12 February 2002
Online at stacks.iop.org/CQG/19/897

Abstract

We report on thermal noise from the internal friction of dielectric coatings made from alternating layers of Ta_2O_5 and SiO_2 deposited on fused silica substrates. We present calculations of the thermal noise in gravitational wave interferometers due to optical coatings, when the material properties of the coating are different from those of the substrate and the mechanical loss angle in the coating is anisotropic. The loss angle in the coatings for strains parallel to the substrate surface was determined from ringdown experiments. We measured the mechanical quality factor of three fused silica samples with coatings deposited on them. The loss angle, $\phi_{\parallel}(f)$, of the coating material for strains parallel to the coated surface was found to be $4.2 \pm 0.3 \times 10^{-4}$ for coatings deposited on commercially polished slides, and $1.0 \pm 0.3 \times 10^{-4}$ for a coating deposited on a superpolished disc. Using these numbers, we estimate the effect of coatings on thermal noise in the initial LIGO and Advanced LIGO interferometers. We also find that the corresponding prediction for thermal noise in the 40 m LIGO prototype at Caltech is consistent with the noise data. These results are complemented by results for a different type of coating, presented in a companion paper.

PACS numbers: 0480, 0480N, 6835G, 6860B, 9555Y

1. Introduction

The experimental effort to detect gravitational waves is entering an important phase. A number of interferometric gravitational wave observatories are being built around the world [1–4] and most should be operational in the next few years. Plans are being developed to operate the next generation of interferometers, and crucial research is going on now to ensure that these interferometers will have the sensitivity necessary to reach distances at which multiple events may be detected per year [5–7].

The sensitivity of interferometric gravitational wave observatories is limited by fundamental noise sources. In Advanced LIGO, thermal noise from the internal degrees of freedom of the interferometer test masses is expected to be the limiting noise source in the middle frequency range (∼30–500 Hz). This is also the interferometer's most sensitive frequency band. Thus, any additional thermal noise, such as thermal noise associated with optical coatings, will directly reduce the number of events that Advanced LIGO can detect.

The initial LIGO interferometer uses fused silica for the interferometer test masses, the beam splitter and other optics. Fused silica has been shown to have very low internal friction [8–10] and will therefore exhibit very low (off-resonance) thermal noise. This property, coupled with the fact that high quality, large, fused silica optics are commercially available, makes fused silica a natural choice for the initial interferometer. Sapphire, which has even lower internal friction [11, 12] (although higher thermoelastic loss), is currently proposed as the material from which to fabricate the optics for use in Advanced LIGO [5]. In addition to lower thermal noise, sapphire offers benefits due to its superior thermal conductivity, which, in transporting heat from the reflective surface of the test masses, allows a higher power laser to be used.

In order to use the test masses as mirrors, optical coatings must be applied to the surface. To obtain high reflectivities, multi-layer, dielectric coatings are used. Such coatings consist of alternating layers of two dielectric materials with differing refractive indices. The number of layers deposited determines the reflectivity. It is possible to use a number of different dielectric material pairs for reflective coatings, but it has been found that coatings made with alternating layers of Ta_2O_5 and SiO_2 give the necessary reflectivity while at the same time satisfying the stringent limits on optical loss and birefringence required for LIGO [13]. However, the effect of these coatings on thermal noise is only now being studied.

The simplest way to predict the thermal noise is to use the fluctuation–dissipation theorem [14]. It states that the thermal noise power spectrum is proportional to the real part of the mechanical admittance of the test mass. Explicitly

$$S_x(f) = \frac{k_B T}{\pi^2 f^2} \mathrm{Re}\{\mathbb{Y}(f)\} \tag{1}$$

where S_x is the spectral density of the thermally induced fluctuations of the test mass surface as read by the interferometer, T is the temperature of the test mass and f is the frequency of the fluctuations. The quantity $\mathbb{Y}(f)$ is the mechanical admittance of the test mass to a cyclic pressure distribution having the same form as the interferometer beam intensity profile [15]. For LIGO, the proposed beam profile is Gaussian. $\mathrm{Re}\{\mathbb{Y}(f)\}$ can be written in terms of the mechanical loss angle, ϕ_{readout}, of the test mass response to the applied cyclic Gaussian pressure distribution. To calculate the thermal noise we must therefore obtain ϕ_{readout}.

The loss angle ϕ_{readout} depends both on the distribution of losses in the test mass and on the shape of the deformation of the test mass in response to the applied pressure. If the distribution of losses in the test mass were homogeneous, the loss angle ϕ_{readout} would be independent of the deformation of the test mass. In that case, one could obtain ϕ_{readout} by measuring the loss angle associated with a resonant mode of the test mass, $\phi = 1/Q$, where Q is the quality factor

of a resonant mode. However, when the distribution of mechanical losses in the test mass is not homogeneous, this approach does not work.

One way of obtaining ϕ_{readout} would be to measure it directly. This would involve applying a cyclic Gaussian pressure distribution to the test mass face and measuring the phase lag of the response. But such an experiment presents several insuperable technical difficulties and is useful mainly as a thought experiment, in which interpretation of the result would be simple.

In this paper, we give the results of another kind of experiment whose results allow us to calculate ϕ_{readout} using elasticity theory. The measurement process is relatively straightforward: we compare the quality factor, Q, of vibrations of an uncoated sample of fused silica to the quality factor when a coating has been applied. In order to make the effect easier to measure, and to improve the accuracy of the measurements, we used thin pieces of fused silica rather than the relatively thick mirrors used in LIGO. Our measurements show a significant reduction of the Q due to mechanical loss associated with the coating.

In choosing to make the measurements easy to carry out, we necessarily complicated the interpretation of the results. Scaling from the results of our measurements to the prediction of ϕ_{readout} takes some effort. In section 2 we describe the relationship between the measured coating loss angle, $\phi_{\parallel}$, and the interferometer readout loss angle, ϕ_{readout}. Section 3 describes the measurement process. The results are given in section 4. The implications for LIGO are described in section 5, and a programme of future work is discussed in section 6. This paper is complemented by a companion paper describing similar measurements on Al_2O_3/Ta_2O_5 coatings [16].

2. Theory

To use the fluctuation–dissipation theorem, equation (1), to predict thermal noise in LIGO, we need to calculate the real part of the mechanical admittance of the test mass. The mechanical admittance of the test mass is defined as

$$\mathbb{Y}(f) \equiv \mathrm{i}2\pi f \frac{x(f)}{F} \tag{2}$$

where F is the (real) amplitude of a cyclic force applied to the test mass at frequency f and $x(f)$ is the amplitude of the steady state displacement response. Choosing the appropriate pressure distribution with which to excite the test mass constitutes the first step in the calculation. Levin [15] has argued that in calculating the thermal noise read by an interferometer, the appropriate pressure distribution has the same profile as the laser beam intensity and should be applied to the test mass face (in the same position and orientation as the beam). In the case of the initial LIGO interferometer, the laser beam has a Gaussian intensity distribution. A Gaussian beam profile is also proposed for Advanced LIGO. The corresponding cyclic pressure distribution is

$$p(\vec{r}, t) = p(r, t) = \frac{2F}{\pi w^2} \exp\left(\frac{-2r^2}{w^2}\right) \sin(2\pi f t) \tag{3}$$

where $\vec{r}$ is a point on the test mass surface, $r = |\vec{r}|$, f is the frequency of interest and w is the field amplitude radius of the laser beam. (At the radius w, the light intensity is $1/e^2$ of maximum.) To simplify the calculation of the response $x(f)$, we make use of the fact that the beam radius is considerably smaller than the test mass radius, and approximate the test mass by an infinite half-space. This allows us to ignore boundary conditions everywhere except on the face of the test mass. For the case of homogeneous loss, Liu and Thorne [17] have shown that this approximation leads to an overestimate of the thermal noise, but that for a test mass of radius 14 cm, the error is about 30% or less for beam field amplitude radii w up to 6 cm.

To calculate the real part of the admittance we follow Levin and rewrite it in the form

$$\mathrm{Re}\{\mathbb{Y}(f)\} = \frac{4\pi f U(f)}{F^2}\phi \tag{4}$$

where $U(f)$ is the maximum elastic energy stored in the test mass as a result of the excitation at frequency f and ϕ is the loss angle of the response. Equation (4) holds at frequencies far below the first resonance of the test mass, provided $\phi \ll 1$, and is obtained as follows. Under the conditions stated

$$U(f) = \tfrac{1}{2}F|x(f)| \tag{5}$$

and the response $x(f)$ to the excitation is

$$x(f) = |x(f)|\exp(-\mathrm{i}\phi) \approx |x(f)|(1 - \mathrm{i}\phi). \tag{6}$$

Substituting equations (5) and (6) into equation (2) and taking the real part yields equation (4).

The strategy is then to calculate $U(f)$ and ϕ under the pressure distribution in equation (3). Calculation of the loss angle ϕ requires some care since the loss angle is specific to the applied force distribution and to the associated deformation. If the material properties or intrinsic sources of loss are not isotropic and homogeneous throughout the sample, different deformations will exhibit different loss angles. Since interferometer test masses do have inhomegeneous loss due to the dielectric coating on the front surface, the calculation of thermal noise depends on obtaining the value of the loss angle associated with precisely the response to the pressure distribution given in equation (3). Throughout this paper we will assume that losses in the substrate are always homogeneous and isotropic and that the only source of inhomogeneous and anisotropic loss is the coating.

The loss angle $\phi \equiv \phi_{\mathrm{readout}}$ associated with the Gaussian pressure distribution can be written as a weighted sum of coating and substrate losses. We will first obtain an expression for the loss angle in the simple case where the coating loss is homogeneous and isotropic, but quickly generalize to anisotropic coating loss.

If the loss in the coating is homogeneous and isotropic, yet different from that of the substrate, we can write

$$\phi_{\mathrm{readout}} = \frac{1}{U}(U_{\mathrm{substrate}}\,\phi_{\mathrm{substrate}} + U_{\mathrm{coating}}\,\phi_{\mathrm{coating}}) \tag{7}$$

where U is the maximum elastic energy stored in the sample as a consequence of the applied pressure, $U_{\mathrm{substrate}}$ is the portion of the energy stored in the substrate, U_{coating} is the portion of the energy stored in the coating, $\phi_{\mathrm{substrate}}$ is the loss angle of the substrate and ϕ_{coating} is the loss angle of the coating. To simplify the calculation of the energies, we make use of the fact that the frequencies where thermal noise dominates interferometer noise budgets are far below the first resonances of the test masses. Thus, the shape of the response of the test mass to a cyclic Gaussian pressure distribution of frequency f is well approximated by the response to an identical Gaussian pressure distribution that is constant in time. Thus, to a good approximation, U, $U_{\mathrm{substrate}}$ and U_{coating} can be calculated from the deformation associated with the *static* Gaussian pressure distribution

$$p(r) = \frac{2F}{\pi w^2}\exp\left(\frac{-2r^2}{w^2}\right). \tag{8}$$

Since we are in the limit where the coating is very thin compared to the width of the pressure distribution

$$U_{\mathrm{coating}} \approx \delta U d \tag{9}$$

where δU is the energy density stored at the surface, integrated over the surface, and d is the thickness of the coating. Similarly, $U_{\text{substrate}} \approx U$, giving

$$\phi_{\text{readout}} = \phi_{\text{substrate}} + \frac{\delta U d}{U}\phi_{\text{coating}}. \tag{10}$$

If, however, the loss angle of the coating is not isotropic, the second term in equation (10) must be expanded. Since the coatings have a layer structure, we cannot ignore the possibility of anisotropy of structural loss in the calculation of thermal noise.

To address the possible anisotropy of the structural loss we shall use the following model. The energy density ρ_U of a material that is cyclically deformed will generally have a number of terms. We shall associate a different (structural) loss angle with each of these terms. For example, in cylindrical coordinates

$$\rho_U = \rho_{rr} + \rho_{r\theta} + \cdots \tag{11}$$

where

$$\begin{aligned} \rho_{rr} &\equiv \tfrac{1}{2}\sigma_{rr}\epsilon_{rr} \\ \rho_{r\theta} &\equiv \tfrac{1}{2}\sigma_{r\theta}\epsilon_{r\theta} \\ &\vdots \end{aligned} \tag{12}$$

where σ_{ij} are the stresses and ϵ_{ij} the strains. The associated loss angles are ϕ_{rr}, $\phi_{r\theta}$, etc. In this paper we will assume that the loss angles associated with energy stored in strains parallel to the plane of the coating are all equal. This assumption is motivated by the observation that many isotropic amorphous materials, like fused silica, do not show significantly different quality factors for many modes even though the relative magnitude of the various terms in the elastic energy varies significantly between the modes [18]. The measurements made at Glasgow and Stanford Universities further strengthen this assumption [16]—those measurements show no significant variation of the coating loss as the relative size of the parallel strain energy terms changes from mode to mode.

Since we will always have traction-free boundary conditions for the problems considered here, we shall always have $\epsilon_{rz} = \epsilon_{zr} = 0$. Thus we will have loss angles associated only with the following coating energy density components:

$$\begin{aligned} \rho'_{U\parallel} &= \tfrac{1}{2}(\epsilon'_{rr}\sigma'_{rr} + \epsilon'_{\theta\theta}\sigma'_{\theta\theta} + \epsilon'_{r\theta}\sigma'_{r\theta}) \\ \rho'_{U\perp} &= \tfrac{1}{2}\epsilon'_{zz}\sigma'_{zz} \end{aligned} \tag{13}$$

where ϵ'_{ij} are the strains and σ'_{ij} the stresses in the coating. We define the loss angle associated with the energy density in parallel coating strains $\rho'_{U\parallel}$, as $\phi_\parallel$, and the loss angle associated with the density of energy in perpendicular coating strains, $\rho'_{U\perp}$, as $\phi_\perp$. The components of the energy density in equation (13) integrated over the surface of the (half-infinite) test mass are

$$\begin{aligned} \delta U_\parallel &= \int_S \rho'_{U\parallel}\,\mathrm{d}^2 r \\ \delta U_\perp &= \int_S \rho'_{U\perp}\,\mathrm{d}^2 r \end{aligned} \tag{14}$$

so that finally, to account for the anisotropic layer structure of the coating, equation (10) is replaced by

$$\phi_{\text{readout}} = \phi_{\text{substrate}} + \frac{\delta U_\parallel d}{U}\phi_\parallel + \frac{\delta U_\perp d}{U}\phi_\perp. \tag{15}$$

To obtain an expression for ϕ_{readout} we need to calculate $\delta U_{\parallel}$, $\delta U_{\perp}$ and U for a coated half-infinite test mass subject to the Gaussian pressure distribution $p(r)$ of equation (8). The quantities $\delta U_{\parallel}$ and $\delta U_{\perp}$ involve only the stress and strain in the coating. The total energy involves the stress and strain throughout the substrate,

$$U = \pi \int_0^\infty \mathrm{d}z \int_0^\infty r\,\mathrm{d}r(\epsilon_{rr}\sigma_{rr} + \epsilon_{\theta\theta}\sigma_{\theta\theta} + \epsilon_{zz}\sigma_{zz} + 2\epsilon_{rz}\sigma_{rz}) \tag{16}$$

where ϵ_{ij} are the strains and σ_{ij} the stresses in the substrate. To obtain the stresses and strains in the coating and in the substrate we must solve the axially symmetric equations of elasticity for the coated half-infinite test mass subject to the pressure distribution $p(r)$. The general solution to these equations for an uncoated half-infinite test mass is given by Bondu *et al* [19] (with corrections by Liu and Thorne [17]).

Because the coating is thin, we can, to a good approximation, ignore its presence in the solution of the elastic equations for the substrate. The strains in the coating should also not vary greatly as a function of depth within the coating, and we shall approximate them as being constant. Due to axial symmetry, $\epsilon_{r\theta} = \epsilon_{\theta r} = \epsilon'_{r\theta} = \epsilon'_{\theta r} = 0$. Due to traction-free boundary conditions, $\epsilon'_{rz} = \epsilon'_{zr} = 0$ at the coating surface, and the same must therefore hold (to leading order) for the entire coating. This approximation is valid, provided the Poisson's ratio of the coating is not very different from that of the substrate. To obtain the non-zero stresses and strains in the coating (ϵ'_{rr}, $\epsilon'_{\theta\theta}$ and ϵ'_{zz}) we note that since the coating is constrained tangentially by the surface of the substrate, the coating must have the same tangential strains (ϵ'_{rr} and $\epsilon'_{\theta\theta}$) as the surface of the substrate. Also, the coating sees the same perpendicular pressure distribution (σ'_{zz}) as the surface of the substrate. These conditions, which represent reasonably good approximations for the case of a thin coating, allow us to calculate all the coating stresses and strains in terms of the stresses and strains in the surface of the substrate. See the appendix for the details of this calculation.

Using the solutions for ϵ'_{ij}, σ'_{ij}, ϵ_{ij} and σ_{ij} derived in the appendix, and substituting into equations (13)–(16), we obtain the required quantities,

$$U = \frac{F^2(1-\sigma^2)}{2\sqrt{\pi}wY} \tag{17}$$

$$\delta U_{\parallel}/U = \frac{1}{\sqrt{\pi}w}\frac{Y'(1+\sigma)(1-2\sigma)^2 + Y\sigma'(1+\sigma')(1-2\sigma)}{Y(1+\sigma')(1-\sigma')(1-\sigma)} \tag{18}$$

$$\delta U_{\perp}/U = \frac{1}{\sqrt{\pi}w}\frac{Y(1+\sigma')(1-2\sigma') - Y'\sigma'(1+\sigma)(1-2\sigma)}{Y'(1-\sigma')(1+\sigma)(1-\sigma)} \tag{19}$$

where Y and σ are the Young's modulus and Poisson's ratio of the substrate, and Y' and σ' are the Young's modulus and Poisson's ratio of the coating. In general, the coating Young's modulus and Poisson's ratio are different in the parallel and perpendicular directions. For the Young's modulus, these values can be found by averaging the Young's moduli of the coating materials, and by averaging the reciprocals of the Young's moduli, respectively [20]. However, because the values for SiO_2 and Ta_2O_5 are similar, the Young's moduli and Poisson's ratios in the two directions are similar. This is in contrast to the case for the ϕ where it is not known whether $\phi_{\parallel}$ is similar in magnitude to $\phi_{\perp}$. For simplicity, we have therefore approximated the Young's moduli and Poisson's ratios in the two directions as equal to the value for stresses parallel to the coating. Thus, from equation (15)

$$\phi_{\text{readout}} = \phi_{\text{substrate}} + \frac{1}{\sqrt{\pi}}\frac{d}{w}\left(\frac{Y'(1+\sigma)(1-2\sigma)^2 + Y\sigma'(1+\sigma')(1-2\sigma)}{Y(1+\sigma')(1-\sigma')(1-\sigma)}\,\phi_{\parallel} + \frac{Y(1+\sigma')(1-2\sigma') - Y'\sigma'(1+\sigma)(1-2\sigma)}{Y'(1-\sigma')(1+\sigma)(1-\sigma)}\,\phi_{\perp}\right). \tag{20}$$

Substituting equations (17) and (20) into equation (4) and substituting the result into the fluctuation–dissipation theorem, equation (1), gives the power spectral density of interferometer test mass displacement thermal noise as

$$S_x(f) = \frac{2k_BT}{\pi^{3/2}f}\frac{1-\sigma^2}{wY}\left\{\phi_{\text{substrate}} + \frac{1}{\sqrt{\pi}}\frac{d}{w}\frac{1}{YY'(1-\sigma'^2)(1-\sigma^2)} \times [Y'^2(1+\sigma)^2(1-2\sigma)^2\phi_\parallel + YY'\sigma'(1+\sigma)(1+\sigma')(1-2\sigma)(\phi_\parallel - \phi_\perp) + Y^2(1+\sigma')^2(1-2\sigma')\phi_\perp]\right\}. \quad (21)$$

Equation (21) is valid provided that most of the loss at the coated surface occurs in the coating materials themselves and is not due to interfacial rubbing between the coating and the substrate, or to rubbing between the coating layers. If a large proportion of the loss is due to rubbing, the coating-induced thermal noise will not be proportional to the coating thickness as indicated in equation (21). Rather, it may be proportional to the number of layers and may be very dependent on the substrate preparation.

The limits of equation (21) agree with the previous results. In the limit that $\phi_\parallel = \phi_\perp$, the YY' term disappears and the result agrees with the result of Nakagawa who has solved the problem for that case by a different method [21]. The limit of equation (21) in the case $Y' = Y$, $\sigma' = \sigma$ and $\phi_\perp = \phi_\parallel$ agrees with the result obtained previously [22],

$$S_x(f) = \frac{2k_BT}{\pi^{3/2}f}\frac{1-\sigma^2}{wY}\left\{\phi_{\text{substrate}} + \frac{2}{\sqrt{\pi}}\frac{(1-2\sigma)}{(1-\sigma)}\frac{d}{w}\phi_\parallel\right\}. \quad (22)$$

For the case of fused silica or sapphire substrates coated with alternating layers of Ta_2O_5 and SiO_2, the Poisson's ratio of the coating may be small enough ($\lesssim 0.25$) that, for likely values of the other parameters, equation (21) is reasonably approximated (within about 30%) by the result obtained by setting $\sigma = \sigma' = 0$,

$$S_x(f) = \frac{2k_BT}{\pi^{3/2}f}\frac{1}{wY}\left\{\phi_{\text{substrate}} + \frac{1}{\sqrt{\pi}}\frac{d}{w}\left(\frac{Y'}{Y}\phi_\parallel + \frac{Y}{Y'}\phi_\perp\right)\right\}. \quad (23)$$

Equation (23) highlights the significant elements of equation (21). It shows that, in order to estimate the thermal noise performance of a particular coating, we must know all of Y, Y', $\phi_\parallel$, and $\phi_\perp$. It also shows that if $\phi_\parallel \approx \phi_\perp$, then the lowest coating-induced thermal noise occurs when the Young's modulus of the coating is matched to that of the substrate. If $Y' \not\approx Y$, one of $\phi_\parallel$ or $\phi_\perp$ will be emphasized and the other de-emphasized. This is particularly worrying for coatings on sapphire substrates, whose high Young's modulus means that for most coatings, $\phi_\perp$ is likely to be the main contributor to the coating thermal noise. Section 3 describes ringdown experiments on coated samples in order to determine $\phi_\parallel$. Unfortunately, we do not obtain $\phi_\perp$ from ringdown experiments of samples with coatings on the surface. Since the coatings experience free boundary conditions, they are not greatly compressed perpendicular to the surface (there will be some small amount of compression due to Poisson's ratio effects). Therefore $\phi_\perp$ cannot be easily measured in such experiments, and no measurement of $\phi_\perp$ exists at the present time. Because of this, we can only obtain very rough estimates of the coating-induced thermal noise. We will set $\phi_\perp = \phi_\parallel$, but the accuracy of our thermal noise estimates will remain unknown until $\phi_\perp$ is measured.

3. Method

In order to estimate the coating loss component $\phi_\parallel$, we made measurements of the loss angles of fused silica samples with and without the Ta_2O_5/SiO_2 high reflective coating used in LIGO.

A standard way of determining the loss angle at the frequency of a particular resonant mode is to measure its ringdown time, τ_n. This allows the calculation of the mode's quality factor Q, through

$$Q \equiv \pi f_n \tau_n \tag{24}$$

where f_n is the frequency of the resonant mode. The loss angle at the resonance frequency is the inverse of the mode's quality factor

$$\phi(f_n) = 1/Q. \tag{25}$$

Because of the free boundary conditions no energy is stored in strains with perpendicular components. The loss angle ϕ_{coated} of a resonating sample after coating is therefore related to the loss angle ϕ_{uncoated} of the same sample before coating by

$$\phi_{\text{coated}} = \phi_{\text{uncoated}} + \frac{\delta\tilde{U}_{\parallel} d}{\tilde{U}} \phi_{\parallel} \tag{26}$$

where $\tilde{U}$ is the energy stored in the resonance. Similarly, as in section 2, the quantity $\delta\tilde{U}_{\parallel}$ is the resonance energy stored in strains having no component perpendicular to the surface

$$\delta\tilde{U}_{\parallel} = \int_S \mathrm{d}^2 r \sum_{i,j\neq z} \rho'_{ij} \tag{27}$$

where S is the coated surface of the sample, z is the direction perpendicular to the surface and

$$\rho'_{ij} = \tfrac{1}{2}\epsilon'_{ij}\sigma'_{ij}. \tag{28}$$

Just as in section 2, $\phi_{\parallel}$ in equation (26) is the loss angle associated with the energy stored in strains in the plane of the coating. Because we assume that all in-plane loss angles are identical, the loss angle $\phi_{\parallel}$ is the same as in section 2, and once measured, can be substituted directly into equation (21).

For each sample resonance that was found, ϕ_{coated} and ϕ_{uncoated} were measured by recording the Q with and without an optical coating, respectively. The quantity $(\delta\tilde{U}_{\parallel} d/\tilde{U})$ was then calculated either numerically or analytically, allowing equation (26) to be solved for $\phi_{\parallel}$ based on the measured values of ϕ_{coated} and ϕ_{uncoated}. The resulting value for $\phi_{\parallel}$ was then substituted into equation (21) to obtain an interferometer thermal noise estimate.

In order to reduce systematic errors in the Q measurements, we took a number of steps to reduce excess loss (technical sources of loss, extrinsic to the sample) [23, 24][6]. All Q were measured in a vacuum space pumped down to at least 1×10^{-5} Torr, and more typically 2×10^{-6} Torr. This reduced mechanical loss from gas damping. During the Q measurements, the samples were hung below a monolithic silica suspension made by alternating a massive bob of silica with thin, compliant, silica fibres. The suspensions and samples are shown in figure 1. (The suspension is of the same style used previously in [10, 24, 25].) The piece of fused silica rod at the top of the suspension is held in a collet which is rigidly connected to the underside of a thick aluminium plate supported by three aluminium columns. Between the piece of rod held in the collet and the sample was a single fused silica isolation bob. Its function was to stop vibrations from travelling between the sample and the aluminium optical table from which it was suspended. The size chosen for the isolation bob depended on the sample, with the heavier sample requiring a larger bob. The two fibres in the suspension were monolithically pulled out of the neighbouring parts using a H_2–O_2 torch. These fibres had a typical diameter of roughly 100–200 μm. The normal modes of the sample were excited using

[6] In the referenced paper, the more general surface loss parameter d_s is used. For coatings, as we have modelled them here, $\mathrm{d}_s\phi_{\text{bulk}} = \mathrm{d}Y'\phi_{\parallel}/Y$.

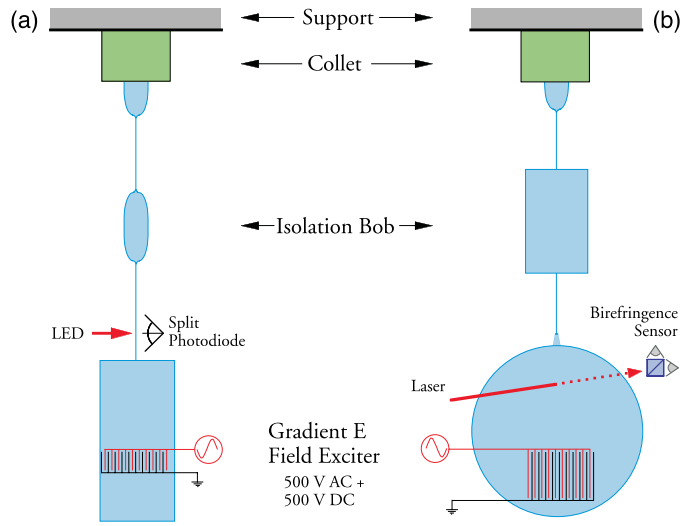

Figure 1. (a) The suspended microscope slide and exciter. (b) The suspended disc and exciter. In both (a) and (b), the entire structure below the steel collet is fused silica.

a comb capacitor [26]. This exciter was made from two copper wires sheathed with Teflon, each having a total diameter of about $1/2$ mm. The two wires were then wrapped around a ground plane and placed about 1 mm from the face of the sample. Special care was taken to ensure that the exciter and the sample did not touch at any point. The position of the exciter is shown in figure 1. Alternating wires of the comb capacitor were given a 500 V dc voltage while the other wires were held at ground to induce a polarization in the glass sample. To reduce any eddy current damping [23] and to reduce the probability that polarized dust could span the gap between the sample and the exciter, the exciter was always kept more than $1/2$ mm away from the sample. An ac voltage at a resonance frequency of the sample was then added to the dc voltage to excite the corresponding mode. Once the mode had been excited ('rung up') to an amplitude where it could be seen clearly above the noise, both the ac and dc voltages were removed and both exciter wires were held at ground. The sample was then allowed to ring down freely.

The amplitude of excitation in the sample was read out using a birefringence sensor [27, 28] or (in the earliest measurements) by a shadow sensor. For the birefringence sensor, a linearly polarized beam is passed through the sample at or near a node of the resonant mode under study. Modally generated stress at the node induces birefringence in the glass, which couples a small amount of the light into the orthogonal polarization, phase shifted by $\pi/2$. Thus, the light exiting the sample is slightly elliptically polarized. The beam is then passed through a $\lambda/4$ wave-plate aligned with the initial polarization. This brings the phases of the two orthogonal polarization components together, converting the elliptically polarized light to a linear polarization that is rotated slightly compared with the initial polarization. The rotation angle is (to first order) proportional to the modal strain, and is measured by splitting the beam with a polarizing beamsplitter and monitoring the relative intensity of light in the two channels. This was done with two identical photodiodes and a differencing current-to-voltage amplifier. The output voltage oscillates sinusoidally at the resonant frequency in proportion to the modally induced strain. This signal is sent to a lock-in amplifier to demodulate it to a lower frequency and the data is collected on a PC. The ringdown time τ_n was obtained

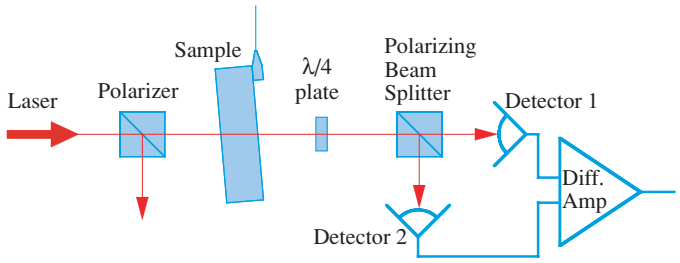

Figure 2. Layout of the birefringence sensor.

by fitting the acquired signal to a damped sinusoid, or by extracting the envelope of the decay. Both approaches yielded the same results, although the accuracy of the former was less sensitive to corruption from noise. A schematic drawing of the optical readout system is shown in figure 2.

For the shadow sensor, an LED is used to cast the shadow of the fused silica suspension fibre onto a split photodiode. The LED/diode pair is positioned close to where the suspension fibre is welded to the edge of the sample. The fibre near the weld point will faithfully follow the motion of the edge of the sample. As the sample resonates, the fibre's shadow moves back and forth on the photodiode at the same frequency. The amount of light falling on each half of the split photodiode changes proportionally. The currents from each half of the photodiode are then compared with a differential current-to-voltage amplifier as in the case of the birefringence sensor. The data acquisition and analysis were identical for both sensors.

For relatively rigid but transparent samples like the ones used here, the birefringence sensor is significantly more sensitive and much easier to use than the shadow sensor. The shadow sensor is better suited to more compliant samples. In both cases, however, the dominant sources of broadband noise were laser noise and noise from the differential amplifier.

The samples were coated by Research Electro-Optics Corporation (REO) of Boulder, Colorado, USA. The coating was a dielectric optical coating consisting of alternating layers of SiO_2 and Ta_2O_5. The coating was laid down using argon ion beam sputtering, followed by annealing at 450 °C. We chose to examine this particular type of coating because it is the one used on the initial LIGO interferometer mirrors that are currently installed at the LIGO sites. This coating is also of the type currently proposed for Advanced LIGO optics.

The first samples we studied were three rectangular prisms in the shape of microscope slides (7.6 cm × 2.5 cm × 0.1 cm) made of Suprasil 2 brand fused silica from Heraeus Quartzglas GmbH of Hannau, Germany. The surface of these samples was treated with a commercial polish to a scratch/dig specification of 80/50. There was no specification on the overall flatness or the surface figure. Two of the three slides (slides A and B) were coated on both sides with a reflective Ta_2O_5/SiO_2 coating of 3% transmittance for normally incident, 1 μm wavelength light. The third slide (slide C) was left uncoated as a control. Slide A was suspended from a corner, which had remained uncoated due to being supported at those points during coating. Therefore, welding the suspension fibre to the corner did not induce visible damage to the coating. Slide B, on the other hand, was suspended from the centre of one of its short edges. During the weld, the coating near the suspension point was visibly damaged in a small crescent shape of radius 2 mm surrounding the suspension point. This damaged region was etched off using hydrofluoric (HF) acid. Table 1 shows the modes and quality factors for which Q were repeatably measured. A preliminary version of these results was reported at the Third Edoardo Amaldi Conference on Gravitational Waves [25].

Table 1. Measured Q for transverse bending modes of the three commercially polished fused silica slides. Slides A and B were coated while slide C was left uncoated as a control.

Slide	Coating	Mode	Frequency (Hz)	Q
A	HR	2	1022	$1.1 \pm 0.5 \times 10^5$
	HR	3	1944	$1.6 \pm 0.1 \times 10^5$
	HR	4	2815	$1.6 \pm 0.1 \times 10^5$
B	HR	2	962	$1.3 \pm 0.1 \times 10^5$
C	None	2	1188	$4.0 \pm 0.2 \times 10^6$
	None	3	2271	$4.9 \pm 0.3 \times 10^6$

After measuring the Q of the slides, we obtained a disc of Dynasil brand fused silica, 164.85 mm in diameter and 19.00 mm thick from Zygo Corporation of Middlefield, Connecticut. In an effort to determine the effect of surface preparation on the loss due to optical coatings, this sample was made with strict specification for surface flatness, scratch/dig and surface roughness. The coated surface had a surface flatness of less than $\lambda/20$ ($\lambda = 633$ nm), a scratch/dig of 60/40 and a surface roughness of less than 4 Å rms. The back surface had a surface flatness of less than $\lambda/6$, a scratch/dig of 60/40, and a surface roughness of less than 4 Å rms. These specifications are nearly as stringent as the actual requirements for LIGO mirrors. To avoid destroying the surface with welding, an 'ear' of fused silica was bonded onto the back surface using hydroxy catalysis bonding (silicate bonding) [29]. This ear is shaped like a rectangular block with a pyramid on one face. One face of the block is bonded to the sample, so that the tip of the pyramid faces radially. This allows the monolithic suspension to be welded with a torch to the tip of the pyramid without heating the sample very much (see figure 3). Once hung, the Q of the sample was measured using the birefringence readout.

Due to the thickness of this sample (required to meet the flatness specification), only one normal mode had a frequency below 5 kHz. The useful bandwidth of the high voltage amplifier that was used to drive the exciter is about 5 kHz, so measurements were possible only on this mode. This was the 'butterfly' mode, with two radial nodal lines ($\ell = 2$) and no circumferential nodal lines ($n = 0$) [30].

After measuring the Q of this uncoated sample, it was sent to REO to be coated. It received a high reflective (HR) coating on one side, having 1 ppm transmittance and optimized for a 45° angle of incidence. The sample was then rehung and the Q remeasured. As can be seen from table 2, the coating caused a significant reduction in the quality factor. To rule out possible excess loss due to the suspension, the sample was then removed and again rehung. During this hanging attempt (between successful hanging numbers 3 and 4 in table 2), the isolation bob fell and sheared off the bonded ear. The bond did not give; rather, material from the sample was pulled out along with the ear. A second ear was rebonded at 180° to the original ear. Unfortunately, this ear was also sheared off in the same way during the attempt to suspend the sample. This time, the source of the break occurred along the bonded surface, although some of the substrate pulled away as well. Finally, a third attempt succeeded with an ear bonded at 90° to the original ear (hanging number 4 in table 2). Despite the broken ears, the quality factor of the coated disc did not change significantly. The results of all Q measurements on the disc are shown in table 2.

Since it is difficult in any measurement of high Q to completely eliminate the extrinsic technical sources of loss (excess loss), the quality factors measured for a given sample varied slightly from mode to mode or within a single mode between different hangings. Since excess loss always acts to reduce the measured Q, the best indicator of the true internal friction of a

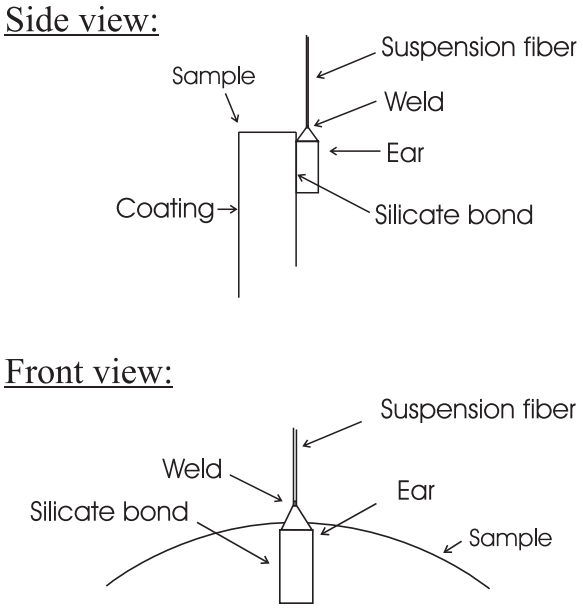

Figure 3. Details of the attachment point. The suspension fibre is welded to the top of the ear. The ear is in turn silicate-bonded along one of its flat faces to the uncoated side of the sample.

Table 2. Measured Q for butterfly mode of the superpolished fused silica disc. In hangings 1 and 2, the disc remained uncoated whereas in hangings 3 and 4 the disc had been coated.

Hanging number	Coating	Frequency (Hz)	Q
1	None	4107	$3.46 \pm 0.02 \times 10^6$
2	None	4107	$3.10 \pm 0.007 \times 10^6$
3	HR (45°)	4108	$1.28 \pm 0.02 \times 10^6$
4[a]	HR (45°)	4121	$1.24 \pm 0.001 \times 10^6$

[a] Ear was sheared off twice before this hanging.

sample is the quality factor of the highest Q mode over all modes and hangings. The spread of measured Q within single hangings was relatively small. For example, the three Q measured in hanging number 2 (sample uncoated) were all between 3.1×10^6 and 2.8×10^6. The twelve Q measured in hanging number 3 (sample coated) were all within 1.28×10^6 to 1.09×10^6. As can be seen from tables 1 and 2, the measured Q also did not vary much between modes or hangings, nor between samples in the case of the two coated slides. The reproducibility of the Q of the disc argues strongly that neither the silicate-bonded ear nor the broken ears affected the loss of the sample. The range of measured Q for nominally similar situations is indicative of the level of the variable excess loss. Thus, for all our samples, the large difference in Q between the coated and the uncoated measurements must be due to the coating, and not to statistical variation, excess loss, nor, in the case of the disc, to the broken ears.

4. Results

Using the procedure described in section 3, we obtained Q values from both the slides and the thick disc. To calculate $\phi_\parallel$ from the measured Q we need to know the value of $\delta\tilde{U}_\parallel d/\tilde{U}$

Table 3. Physical parameters of the coating and samples. These values are used to calculate the coating loss $\phi_\parallel$ from equation (26).

Sample	Parameter	Value	Units
Slide	Coating layers	14	
	Coating thickness d	2.4	μm
Disc	Coating layers	38	
	Coating thickness d	24.36	μm
Both	Substrate Young's modulus (Y)	7.0×10^{10}	N m^{-2}
	Coating Young's modulus (Y')	1.1×10^{11}	N m^{-2}

for each measured mode of the samples. For transverse bending of the slides, the strain is approximately

$$\epsilon_{ij}(\vec{r}) = \begin{cases} \frac{\partial^2 u_y(z)}{\partial z^2} y & i = j = z \\ 0 & \text{otherwise} \end{cases} \tag{29}$$

where z is the coordinate in the slides' longest dimension, y is the coordinate in the slides' shortest dimension with the origin in the centre plane of the slide and $u_y(z)$ is the transverse displacement of (the centre plane of) the slides due to the bending. Displacements in directions other than y are zero for the transverse bending modes. Using equations (27) and (28) and the coating parameters given in table 3, we find

$$\left[\frac{\delta \tilde{U}_\parallel d}{\tilde{U}}\right]_{\text{slide}} = 7.2 \times 10^{-3} \tag{30}$$

for all transverse bending modes of the slides. The butterfly mode of the disc is more complex, and an analytical expression for strain amplitude $\epsilon(\vec{r})$ was not found. We made a finite-element analysis (FEA) model of this sample and calculated $\tilde{U}_{\text{coating}}/\tilde{U}$ numerically. Details of the FEA analysis are given in the companion paper [16]. This resulted in a value of

$$\left[\frac{\delta \tilde{U}_\parallel d}{\tilde{U}}\right]_{\text{disc}} \approx \left[\frac{\tilde{U}_{\text{coating}}}{\tilde{U}}\right]_{\text{disc}} = 5.3 \times 10^{-3} \tag{31}$$

for the butterfly mode of the disc.

The quantities needed to calculate ϕ_{coated} from equation (26) are shown in table 3. Substituting the Q measurements from table 1 into equation (25) to get the loss angles, then using equation (30) and the values in table 3 in equation (26) and solving for $\phi_\parallel$, we get

$$\phi_{\parallel,\text{slide}} = 4.2 \pm 0.3 \times 10^{-4}. \tag{32}$$

Similarly, from equation (31) and the disc Q in table 2 we get

$$\phi_{\parallel,\text{disc}} = 1.0 \pm 0.3 \times 10^{-4}. \tag{33}$$

The agreement in order of magnitude between these two measured values for $\phi_\parallel$ sets a scale for coating thermal noise. This allows us to make rough estimates of the effect of coating thermal noise on Advanced LIGO. The value of $\phi_\parallel$ for the polished disc agrees within its uncertainty with the value measured for coating loss by the Glasgow/Stanford experiment [16], despite the use of a different coating material in that experiment (Ta_2O_5/Al_2O_3 as opposed to Ta_2O_5/SiO_2). This suggests that the substrate surface polish, which is of similar quality on the disc and on the Glasgow/Stanford samples but less good on the slides, may be an important factor contributing to the loss.

Table 4. Comparison of structural thermal noise with and without taking coatings into account. The effective quality factor $Q_{\rm eff}$ (equal to the reciprocal of $\phi_{\rm readout}$) represents the quality factor a homogeneous mirror would need to have to give the same structural contribution to thermal noise as the actual coated mirror. (The effect of thermoelastic damping, important for sapphire, is not included in $Q_{\rm eff}$.) The final column shows the strain amplitude thermal noise at 100 Hz in the Advanced LIGO interferometer resulting from structural loss in the test mass coatings and substrates.

Test mass material	Coating loss	$Q_{\rm eff}(=1/\phi_{\rm readout})$	Structural thermal noise at 100 Hz, $\sqrt{S_h}$
Sapphire	None	200×10^6	1×10^{-24}
	$\phi_\parallel = 1 \times 10^{-4}$	22×10^6	2×10^{-24}
	$\phi_\parallel = 4 \times 10^{-4}$	6×10^6	4×10^{-24}
Fused silica	None	30×10^6	6×10^{-24}
	$\phi_\parallel = 1 \times 10^{-4}$	18×10^6	7×10^{-24}
	$\phi_\parallel = 4 \times 10^{-4}$	8×10^6	9×10^{-24}

5. Implications

Using equation (23) for the thermal noise due to the coated mirrors, we can now estimate the thermal noise spectrum of the Advanced LIGO interferometer. We calculated the range of coating thermal noise in the pessimistic case using the $\phi_\parallel = 4 \times 10^{-4}$ (from the slide results) and in the more optimistic case using $\phi_\parallel = 1 \times 10^{-4}$ (from the disc result). In both cases, we assumed a beam spot size of 5.5 cm, which is the maximum obtainable on fused silica when limited by thermal lensing effects [31]. We have extrapolated our results to sapphire substrates using the known material properties of sapphire, even though we did not measure coating loss directly on sapphire. (There have been recent measurements of $\phi_\parallel$ for REO coatings deposited on sapphire [32]. Those results are in rough agreement with the measurements described here.) As mentioned before, the thermal noise estimates will be least accurate for sapphire substrates because sapphire coating thermal noise is likely to be dominated by $\phi_\perp$ which has not been measured. The Young's modulus of sapphire is considerably higher than both Ta_2O_5 and SiO_2 in bulk, so the coating Young's modulus is considerably less than sapphire's. For the purposes of estimating coating thermal noise, we will set the Young's moduli and Poisson's ratios in the two perpendicular directions equal, taking them to be the average of the SiO_2 and Ta_2O_5 values.

Table 4 compares the thermal noise estimates for the four cases considered (optimistic estimates and pessimistic estimates on both fused silica and sapphire substrates) to the thermal noise estimates when coatings are not taken into account. The corresponding noise spectra for Advanced LIGO are shown in figures 4 and 5. These were generated using the program `BENCH`[7] `1.13` and show both the total noise and the contribution from the test mass thermal noise. The curves for the total noise were generated using the noise models and parameters from the Advanced LIGO systems design document [31]. The figures show that coating thermal noise is a significant source of noise in the frequency band ∼30–400 Hz for fused silica test masses and ∼40–500 Hz for sapphire test masses.

These estimates are only preliminary indications of the level of coating-induced thermal noise. The largest source of uncertainty is that no measurement has been made of $\phi_\perp$. Also,

[7] The program `BENCH` is available at http://gravity.phys.psu.edu/Bench/. Note: The contribution from structural internal thermal noise in `BENCH 1.12` was found to be erroneously low by a factor of 2. This error has been corrected in versions of `BENCH 1.13` (Aug. 2001) and higher.

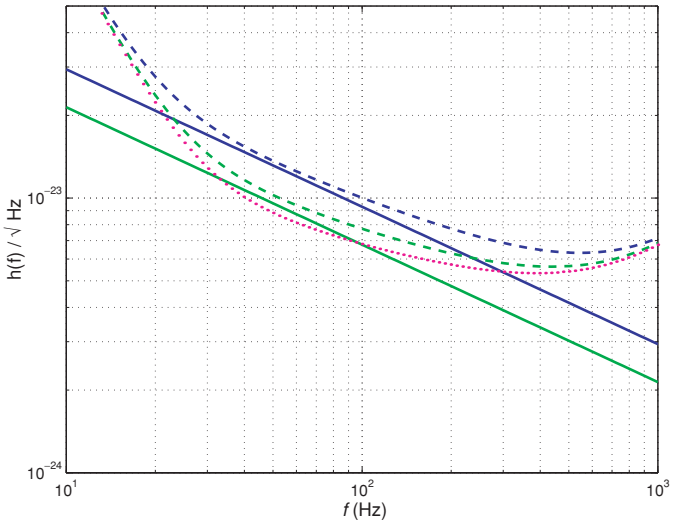

Figure 4. Strain spectrum for Advanced LIGO with fused silica mirrors. The solid, straight lines represent the test mass thermal noise; the dashed curves show the total interferometer noise. The lighter curves were generated using optimistic assumptions including $\phi_{\parallel} = 1 \times 10^{-4}$. The darker curves were generated using pessimistic assumptions including $\phi_{\parallel} = 4 \times 10^{-4}$. The curve shown with a dotted line is the Advanced LIGO noise curve without coating noise as modelled in the Advanced LIGO system design document. In each case, the parameters have been optimized for binary neutron star inspiral.

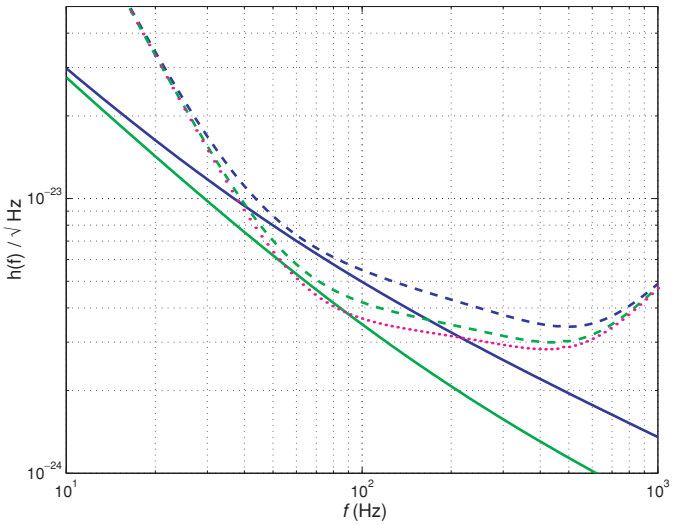

Figure 5. Strain spectrum for Advanced LIGO with sapphire mirrors. The solid, straight lines represent the test mass thermal noise; the dashed curves show the total interferometer noise. The lighter curves were generated using optimistic assumptions including $\phi_{\parallel} = 1 \times 10^{-4}$. The darker curves were generated using pessimistic assumptions including $\phi_{\parallel} = 4 \times 10^{-4}$. The curve shown with a dotted line is the Advanced LIGO noise curve without coating noise as modelled in the Advanced LIGO system design document. In each case, the parameters have been optimized for binary neutron star inspiral.

the Young's modulus of the coating material has not been definitively measured. The half-infinite test mass approximation adds further uncertainty, and this estimate needs to be refined by taking the finite size of the coated test mass into account. In addition, there remains the possibility that the loss associated with the different terms in the energy density $\rho_{\parallel}$ are not equal as supposed here. However, if this were the case, the apparent consistency of the loss between different modes of the samples measured at Glasgow and Stanford [16] would be spurious.

We have also examined the effect of coating thermal noise on the expected sensitivity of the initial LIGO interferometers that are currently being commissioned. In the initial LIGO interferometer, shot noise will be greater than in Advanced LIGO and seismic noise will be significant up to about 40 Hz. Due to the higher level of these other noise sources, test mass thermal noise was not expected to be a large contributor to the total noise [1]. The addition of coating thermal noise raises the overall noise in the most sensitive frequency band, around 200 Hz, by only 4% . Thus, coating thermal noise should not significantly impact the sensitivity of the initial LIGO interferometer.

In addition to the interferometers used for gravitational wave detection, there are a number of prototype interferometers within the gravitational wave community. We have examined data from one of these—the 40 m prototype located at Caltech [33]. In this interferometer, the beam spot size was 0.22 cm and the highest Q seen for a mirror mode was $Q_{\max} = 8.1 \times 10^6$ [34]. Using equation (23) with $\phi_{\parallel} = \phi_{\perp} = 1 \times 10^{-4}$ and $\phi_{\text{substrate}} = 1/Q_{\max}$ in equation (23) yields a predicted thermal noise of $\sim 2 \times 10^{-19}\,\text{m}/\sqrt{\text{Hz}}$ at 300 Hz. This is consistent with the 40 m interferometer noise floor shown in figure 3 of [33]. Coating thermal noise is therefore a possible explanation for the broadband excess noise seen between 300 and 700 Hz. The effect of coating thermal noise is also being explored in the Glasgow 10 metre prototype, the thermal noise interferometer (TNI) at Caltech [35] and in the LASTI prototype at MIT.

6. Future work

The measurements and predictions described here indicate that mechanical loss associated with dielectric optical coatings may be a significant source of thermal noise in Advanced LIGO. Plans are under way for experiments that will allow us to better understand and, perhaps, reduce the coating thermal noise. A programme of loss measurements on various optical coatings deposited on both fused silica and sapphire substrates has begun so that the most appropriate coating may be found. There are also plans to try and correlate the loss angle of the coating with other methods of interrogating its structure. To improve the coating thermal noise without major changes to the optics, the coating loss must be reduced. Study of different dielectric materials is clearly warranted, and changes in the deposition process or post-deposition annealing may also lead to improvements. An agreement has been reached between the LIGO laboratory and two optical coating companies to engage in such research.

Two main models exist for understanding the source of the excess loss in the coating. One is that the internal friction of the coating materials, thin layers of Ta_2O_5 and SiO_2, is high. The other model is that the excess damping comes from rubbing between the layers, and between the coating and the substrate. Experiments are under way to test these models.

Measurement of the unknown parameters in equation (21) are crucial. As discussed in section 2, ringdown Q measurements cannot determine $\phi_{\perp}$ due to the boundary conditions on the free vibration of a sample. A variation of the anelastic aftereffect experiment [28], which will measure the relaxation rate of the coating after being stressed perpendicularly to the

substrate, is being pursued at Caltech [36]. This experiment should give a direct measurement of $\phi_\perp$. The same apparatus is also being used to measure the Young's modulus of the coating.

As seen in equation (21), the coating thermal noise in an interferometer is a strong function of the laser spot size. Increasing the size of the laser spot reduces the contribution from coatings to the total thermal noise, so large spot sizes are desirable. Large spots also help decrease the effect of thermoelastic damping in sapphire mirrors [37], so configurations to increase the spot size are already being considered. A spot size of about 6 cm is the largest that can be achieved on the 25 cm diameter test masses while still keeping the power lost due to diffraction below ∼15 ppm. In the case of 25 cm diameter fused silica test masses, the largest spot size that can be achieved is about 5.5 cm, limited by thermal lensing [31]. Larger diameter test masses and correspondingly larger spot sizes would be one way of reducing the coating-induced thermal noise in Advanced LIGO. However, this would require a re-evaluation of a number of Advanced LIGO subsystems.

Acknowledgments

We would like to thank H Armandula and J Camp for their help in getting our samples coated. We thank L Samuel Finn and everyone who contributed to `BENCH` for making it available to us. F Raab first suggested that we look at the 40 m prototype noise data, and we had useful discussions about the 40 m prototype with D Shoemaker, M Zucker, P Fritschel and S Whitcomb. P Fritschel also showed us how to optimize `BENCH` for maximum binary neutron star reach and helped in getting the large disc sample coated. P Willems provided thoughtful comments on the limits of applicability of the coating loss model. We thank E Gustafson for useful discussions about experiments with fused silica. The Syracuse University glassblower, J Chabot, gave crucial help by teaching us about glass welding. We thank M Mortonson for help in the lab, and E S Watkins for useful comments on the manuscript. This work was supported by Syracuse University, US National Science Foundation grant nos PHY-9900775 and PHY-9210038, the University of Glasgow and PPARC.

Appendix. Stresses and strains in the coating

We obtain the stresses and strains in the coating in terms of the stresses and strains in the surface of the substrate by utilizing the thin coating approximation, and assuming that the coating Poisson's ratio is not very different from that of the substrate. Denoting strains by ϵ_{ij} and stresses by σ_{ij}, this can be summarized in terms of the following constraints. In cylindrical coordinates

$$\epsilon'_{rr} = \epsilon_{rr} \qquad \epsilon'_{\theta\theta} = \epsilon_{\theta\theta} \qquad \epsilon'_{rz} = \epsilon_{rz} \qquad \sigma'_{zz} = \sigma_{zz} \qquad \sigma'_{rz} = \sigma_{rz} \tag{A1}$$

where primed quantities refer to the coating and the unprimed quantities refer to the surface of the substrate. Due to axial symmetry $\epsilon'_{r\theta} = \epsilon'_{z\theta} = \sigma'_{r\theta} = \sigma'_{z\theta} = 0$. We use the following relations, valid for axially symmetric deformations [19]:

$$\begin{aligned}
\sigma_{rr} &= (\lambda + 2\mu)\epsilon_{rr} + \lambda\epsilon_{\theta\theta} + \lambda\epsilon_{zz} \\
\sigma_{\theta\theta} &= \lambda\epsilon_{rr} + (\lambda + 2\mu)\epsilon_{\theta\theta} + \lambda\epsilon_{zz} \\
\sigma_{zz} &= \lambda\epsilon_{rr} + \lambda\epsilon_{\theta\theta} + (\lambda + 2\mu)\epsilon_{zz} \\
\sigma_{rz} &= 2\mu\epsilon_{rz}
\end{aligned} \tag{A2}$$

where λ and μ are the Lamé coefficients. In terms of Young's modulus and Poisson's ratio, the Lamé coefficients are

$$\lambda = Y\sigma/((1+\sigma)(1-2\sigma)) \qquad \mu = Y/(2(1+\sigma)). \tag{A3}$$

Combining equations (A1) and equations (A2), we obtain the stresses and strains in the coating in terms of the stresses and strains in the surface of the substrate,

$$\begin{aligned}
\epsilon'_{rr} &= \epsilon_{rr} \\
\epsilon'_{\theta\theta} &= \epsilon_{\theta\theta} \\
\epsilon'_{zz} &= \frac{\lambda - \lambda'}{\lambda' + 2\mu'}(\epsilon_{rr} + \epsilon_{\theta\theta}) + \frac{\lambda + 2\mu}{\lambda' + 2\mu'}\epsilon_{zz} \\
\epsilon'_{rz} &= \epsilon_{rz} \\
\sigma'_{rr} &= (\lambda' + 2\mu')\epsilon_{rr} + \lambda'\epsilon_{\theta\theta} + \lambda'\epsilon'_{zz} \\
\sigma'_{\theta\theta} &= \lambda'\epsilon_{rr} + (\lambda' + 2\mu')\epsilon_{\theta\theta} + \lambda'\epsilon'_{zz} \\
\sigma'_{zz} &= \sigma_{zz} \\
\sigma'_{rz} &= \sigma_{rz}
\end{aligned} \tag{A4}$$

where λ' and μ' are the Lamé coefficients of the coating, and λ and μ are the Lamé coefficients of the substrate.

We obtain the stresses and strains in the substrate ϵ_{ij}, σ_{ij} from the general solutions to the axially symmetric equations of elasticity for an infinite half-space [17, 19],

$$\begin{aligned}
u_r(r, z) &= \int_0^\infty \left[\alpha(k) - \frac{\lambda + 2\mu}{\lambda + \mu}\beta(k) + \beta(k)kz\right] \mathrm{e}^{-kz} J_1(kr)k \,\mathrm{d}k \\
u_z(r, z) &= \int_0^\infty \left[\alpha(k) + \frac{\mu}{\lambda + \mu}\beta(k) + \beta(k)kz\right] \mathrm{e}^{-kz} J_0(kr)k \,\mathrm{d}k \\
u_\theta(r, z) &= 0 \qquad \text{(axial symmetry)}
\end{aligned} \tag{A5}$$

where $u_r(r, z)$ is the radial deformation of the test mass, $u_z(r, z)$ is the deformation of the test mass perpendicular to the face (z being positive inward) and $u_\theta(r, z)$ is the transverse displacement. $J_1(kz)$ and $J_0(kz)$ are Bessel functions of the first kind. The functions $\alpha(k)$ and $\beta(k)$ are determined by the boundary conditions at the front face: $\sigma_{rz}(r, z = 0) = 0$ and $\sigma_{zz}(r, z = 0) = p(r)$ [19]. Using the pressure distribution $p(r)$ from equation (8) gives

$$\alpha(k) = \beta(k) = \frac{F}{4\pi\mu k} \exp\left(-\frac{1}{8}k^2w^2\right). \tag{A6}$$

Substituting equation (A6) into equations (A5) and performing the integrals leads to

$$u_r(r, z = 0) = -\frac{F(\omega)}{4\pi(\lambda + \mu)r}\left[1 - \exp\left(-\frac{2r^2}{w^2}\right)\right] \tag{A7}$$

$$u_z(r, z = 0) = \frac{F(\omega)(\lambda + 2\mu)}{2\sqrt{2\pi}(\lambda + \mu)\mu w} \exp\left(-\frac{r^2}{w^2}\right) I_0\left(\frac{r^2}{w^2}\right) \tag{A8}$$

where I_0 is a modified Bessel function of the first kind. These deformations are shown, along with the pressure distribution $p(r)$, in figure 6. The strains in the substrate are obtained from the relations

$$\epsilon_{rr} = \delta u_r/\delta r \qquad \epsilon_{\theta\theta} = u_r/r \qquad \epsilon_{zz} = \delta u_z/\delta z \qquad \epsilon_{rz} = (\delta u_z/\delta r + \delta u_r/\delta z)/2. \tag{A9}$$

These strains can now be used to find the stresses in the surface of the substrate through equations (A2), and then to find the stresses and strains in the coating through equations (A4).

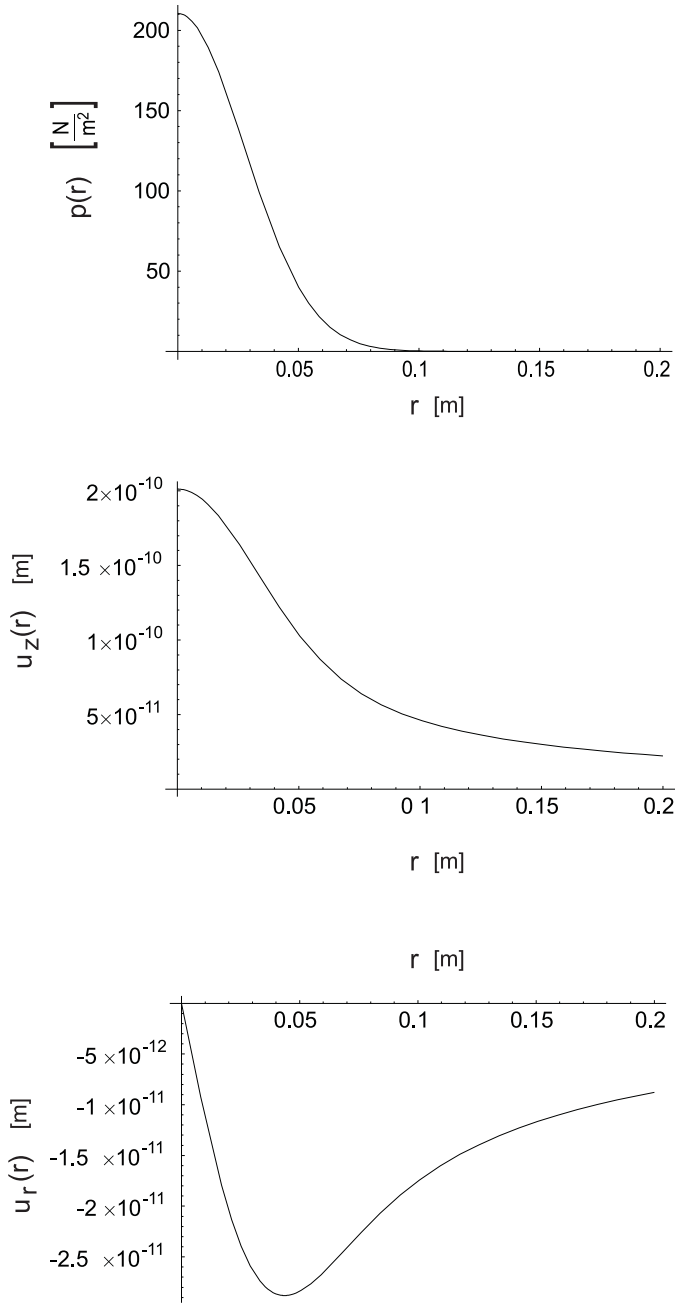

Figure 6. *Top*: Pressure distribution $p(r)$ from equation (8) (with F set to unity). The pressure distribution has the same shape as the laser intensity. *Centre*: The resulting response of the surface in the axial direction, $u_z(r)$. The impression is wider than the applied pressure. *Bottom*: The resulting response in the radial direction, $u_r(r)$. As expected, the surface is pulled towards the centre.

The results for the surface of the substrate are

$$\begin{aligned}
\epsilon_{rr} &= \frac{F}{4\pi(\lambda+\mu)}\left(\frac{1}{r^2}\left(1-\mathrm{e}^{-2r^2/w^2}\right)-\frac{4}{w^2}\,\mathrm{e}^{-2r^2/w^2}\right)\\
\epsilon_{\theta\theta} &= -\frac{F}{4\pi(\lambda+\mu)}\left(\frac{1}{r^2}\left(1-\mathrm{e}^{-2r^2/w^2}\right)\right)\\
\epsilon_{zz} &= -\frac{F}{4\pi(\lambda+\mu)}\left(\frac{4}{w^2}\,\mathrm{e}^{-2r^2/w^2}\right)\\
\epsilon_{rz} &= 0\\
\sigma_{rr} &= \frac{F}{2\pi(\lambda+\mu)}\left(\frac{\mu}{r^2}\left(1-\mathrm{e}^{-2r^2/w^2}\right)-\frac{4(\lambda+\mu)}{w^2}\,\mathrm{e}^{-2r^2/w^2}\right)\\
\sigma_{\theta\theta} &= -\frac{F}{2\pi(\lambda+\mu)}\left(\frac{\mu}{r^2}\left(1-\mathrm{e}^{-2r^2/w^2}\right)+\frac{4\lambda}{w^2}\,\mathrm{e}^{-2r^2/w^2}\right)\\
\sigma_{zz} &= -\frac{F}{2\pi}\left(\frac{4}{w^2}\,\mathrm{e}^{-2r^2/w^2}\right)\\
\sigma_{rz} &= 0
\end{aligned} \tag{A10}$$

and for the coating

$$\begin{aligned}
\epsilon'_{rr} &= \epsilon_{rr}\\
\epsilon'_{\theta\theta} &= \epsilon_{\theta\theta}\\
\epsilon'_{zz} &= -\frac{F(2(\lambda+\mu)-\lambda')}{4\pi(\lambda+\mu)(\lambda'+2\mu')}\left(\frac{4}{w^2}\,\mathrm{e}^{-2r^2/w^2}\right)\\
\epsilon'_{rz} &= 0\\
\sigma'_{rr} &= \frac{F}{2\pi(\lambda+\mu)(\lambda'+2\mu')}\left(\frac{\mu'(\lambda'+2\mu')}{r^2}\left(1-\mathrm{e}^{-2r^2/w^2}\right)\right.\\
&\qquad\left.-\frac{4(\lambda'(\lambda+\mu)+2\mu'(\lambda'+\mu'))}{w^2}\,\mathrm{e}^{-2r^2/w^2}\right)\\
\sigma'_{\theta\theta} &= -\frac{F}{2\pi(\lambda+\mu)(\lambda'+2\mu')}\left(\frac{\mu'(\lambda'+2\mu')}{r^2}\left(1-\mathrm{e}^{-2r^2/w^2}\right)\right.\\
&\qquad\left.+\frac{4(\lambda'(\lambda+\mu+\mu'))}{w^2}\,\mathrm{e}^{-2r^2/w^2}\right)\\
\sigma'_{zz} &= \sigma_{zz}\\
\sigma'_{rz} &= 0.
\end{aligned} \tag{A11}$$

Equations (A10) can now be used to find the energy density in the substrate and integrated over the half-infinite volume, equation (16), to give the total energy in the substrate, equation (17). Equations (A11) can be substituted into the expression for the energy density at the surface, equation (13), and integrated over the surface to give the expressions for $\delta U_{\parallel}$ and $\delta U_{\perp}$ in equations (18) and (19).

References

[1] Abramovici A *et al* 1992 *Science* **256** 325
[2] Giazotto A 1998 *Nucl. Instrum. Methods Phys. Res.* A **289** 518
[3] Lück H *et al* 2000 *Proc. 3rd Edoardo Amaldi Conf. on Gravitational Waves* ed S Meshkov (Melville, NY: AIP) p 119

[4] Tsubono K 1995 *Gravitational Wave Experiments Proc. 1st Edoardo Amaldi Conf.* (Singapore: World Scientific) p 112
[5] LSC white paper on detector research and development webpage http://www.ligo.caltech.edu/docs/T/T990080-00.pdf
[6] *Internal Report* Max-Planck Institut für Quantenoptik, D-85748 Garching 2000
[7] Kuroda K *et al* 1999 *Int. J. Mod. Phys.* D **8** 557 webpage http://www.icrr.u-tokyo.ac.jp/gr/LCGT.pdf
[8] Fraser D B 1968 *J. Appl. Phys.* **39** 5868
Fraser D B 1970 *J. Appl. Phys.* **41** 6
[9] Lunin B S, Torbin S N, Danachevskaya M N and Batov I V 1994 *Moscow State Chem. Bull.* **35** 24
[10] Penn S D, Harry G M, Gretarsson A M, Kittelberger S E, Saulson P R, Schiller J J, Smith J R and Swords S O 2001 *Rev. Sci. Instrum.* **72** 3670
(Penn S D, Harry G M, Gretarsson A M, Kittelberger S E, Saulson P R, Schiller J J, Smith J R and Swords S O 2000 *Preprint* gr-qc/0009035)
[11] Rowan S, Cagnoli G, Sneddon P, Hough J, Route R, Gustafson E K, Fejer M M and Mitrofanov V 2000 *Phys. Lett.* A **265** 5
[12] Braginsky V B, Mitrofanov V P and Panov V I 1985 *Systems with Small Dissipation* (Chicago, IL: University of Chicago Press)
[13] Whitcomb S 1996 *Proc. TAMA Int. Workshop on Gravitational Wave Detection* ed K Tsubono (Tokyo: Universal Academy)
[14] Callen H B and Greene R F 1952 *Phys. Rev.* **86** 703
[15] Levin Yu 1998 *Phys. Rev.* D **57** 659
[16] Crooks D *et al* 2002 *Class. Quantum Grav.* **19** 882
[17] Liu Y T and Thorne K S 2000 *Phys. Rev.* D **62** 122002
[18] Numata K, Bianc G B, Ohishi N, Sekiya A, Otsuka S, Kawabe K, Ando M and Tsubono K 2000 *Phys. Lett.* A **276** 37
[19] Bondu F, Hello P and Vinet J 1998 *Phys. Lett.* A **246** 227
[20] Jones R M 1999 *Mechanics of Composite Materials* (Philadelphia: Taylor and Francis)
[21] Nakagawa N 2001 Oral presentation at the *LIGO Scientific Collaboration Meeting* (*Hanford, WA, USA, 13–16 Aug. 2001*)
[22] Nakagawa N, Gretarsson A M, Gustafson E K and Fejer M M *Phys. Rev.* D at press
(Nakagawa N, Gretarsson A M, Gustafson E K and Fejer M M 2001 *Preprint* gr-qc/0105046)
[23] Huang Y L and Saulson P R 1998 *Rev. Sci. Instrum.* **69** 544
[24] Gretarsson A M and Harry G M 1999 *Rev. Sci. Instrum.* **70** 4081
(Gretarsson A M and Harry G M 1999 *Preprint* physics/9904015)
[25] Gretarsson A M, Harry G M, Penn S D, Saulson P R, Schiller J J and Startin W J 2000 *Proc. 3rd Edoardo Amaldi Conf. on Gravitational Waves* ed S Meshkov (Melville, NY: AIP)
(Gretarsson A M, Harry G M, Penn S D, Saulson P R, Schiller J J and Startin W J 1999 *Preprint* physics/9911040)
[26] Cadez A and Abramovici A 1988 *J. Phys. E: Sci. Instrum.* **21** 453
[27] Startin W J, Beilby M A and Saulson P R 1998 *Rev. Sci. Instrum.* **69** 3681
[28] Beilby M A, Saulson P R and Abramovici A 1998 *Rev. Sci. Instrum.* **69** 2539
[29] Gwo D H 1998 *Proc. SPIE-Int. Soc. Opt. Eng.* **3435** 136
[30] Blevins R D 1979 *Formulas for Natural Frequency and Mode Shape* (New York: Van Nostrand-Reinhold) p 240
[31] Fritschel P *Advanced LIGO Systems Design* webpage www.ligo.caltech.edu/docs/T/T010075-0.pdf
[32] Rowan S 2001 Oral presentation at *Aspen Winter Conf. on Gravitational Waves* (*Aspen, Colorado, USA, 4–10 Feb. 2001*)
[33] Abramovici A *et al* 1996 *Phys. Lett.* A **218** 157
[34] Gillespie A and Raab F 1995 *Phys. Rev.* D **52** 577
[35] Libbrecht K 2001 California Institute of Technology Private communication
[36] Willems P 2001 California Institute of Technology Private communication
[37] Braginksy V B, Gorodetsky M L and Vyatchanin S P 1999 *Phys. Lett.* A **264** 1